Kinetics of the Lamellar–Inverse Hexagonal Phase Transition Determined by Time-Resolved X-ray Diffraction†

Mark W. Tate, Erramilli Shyamsunder, and Sol M. Gruner*
Department of Physics, Princeton University, Princeton, New Jersey 08544
Kevin L. D'Amico
Exxon Research and Engineering Company, Annandale, New Jersey 08801
Received July 25, 1991; Revised Manuscript Received October 21, 1991

ABSTRACT: The kinetics of the lamellar (L_α)–inverse hexagonal (H_{II}) phase transition in diacylphosphatidylethanolamine (PE)–water systems were probed with time-resolved X-ray diffraction. Transition kinetics in the fast time regime (~100 ms) were studied by initiating large temperature jumps (up to 30 °C) with a 50-ms electrical current pulse passed through a lipid–salt water dispersion, resulting in ohmic heating of the sample. Diffraction with a time resolution to 10 ms was acquired at the National Synchrotron Light Source. The time constant for the phase transition for 1,2-dioleoyl-*sn*-glycero-3-phosphoethanolamine (DOPE) was on the order of 100 ms for the largest temperature jumps recorded. Faster transition behavior was found for a 1,2-dielaidoyl-*sn*-glycero-3-PE mixture. The H_{II} lattice parameters for both systems were seen to swell from an initial value commensurate with the lamellar lattice to the final equilibrium value. The rate of swelling was seen to be independent of the magnitude of the temperature jump. For small temperature jumps (<10 °C), the phase transition kinetics slow dramatically, and transition studies can readily be performed on a conventional rotating anode X-ray source. At 4 °C, a DOPE sample was observed to slowly convert to the hexagonal phase over the course of a week, with the decay in the lamellar intensity fitting a power law behavior over four decades of time. This power law behavior is shown to have interesting consequences to the determination of the phase transition temperature of lipid–water dispersions by conventional methods such as calorimetry.

The cell membrane is composed of a large variety of phospholipid species, roughly 10–50% of which will form a nonbilayer phase when isolated from the other membrane constituents (Cullis et al., 1985). One role proposed for the inclusion of these nonbilayer lipid species into the bilayer membrane is to facilitate the formation of the transient nonbilayer structures which occur during various cellular functions (Ellens et al., 1989). Little is known about the dynamics of formation of these structures, however. Hopefully, the basis for understanding the changes in membrane morphology that accompany various cell processes can be established by studying structural phase transitions in well-defined systems.

The amphiphilic nature of the lipid molecule dictates the basic organizational principle of the lipid when mixed with water. The lipid has a polar headgroup which prefers the polar environment provided by water. The nonpolar hydrocarbon chains, by contrast, aggregate to minimize contact with the polar solvent, resulting in structures in which the headgroups form a continuous interface between the hydrocarbon chains and water. Two commonly seen mesophases which satisfy these conditions are the lamellar (L_α)[1] and the inverse hexagonal (H_{II}) phases (Figure 1). The L_α phase consists of alternating planar regions of lipid and water. The H_{II} phase consists of cylindrical rods of water arranged on a hexagonal lattice. The water region is surrounded by the polar headgroup with the hydrocarbon tails filling the interstitial regions of the lattice.

Since these two phases are of different topologies, the phase transition between the two must involve tearing and reorganization within the lipid monolayer. The cost in free energy of exposing the hydrocarbon region to water is quite high, imposing a large kinetic barrier to the transition. L_α–H_{II} phase transitions in many systems do indeed occur quite slowly, often taking anywhere from several minutes to days to occur for changes in temperature less than 5 °C. The large hysteresis seen in the phase transition temperature is another indication of its slow nature. Our X-ray data show that coexisting phases under such slow transition conditions exhibit well-ordered lattices throughout the transition period (see Results). This indicates that the material within the sample can reorder much more quickly than the transition time and suggests that it is the large kinetic activation barrier which limits the transition in this regime. A systematic study of the transition rates under small perturbation to the system serves as a probe of this barrier.

To probe the mechanisms of the transition, one must increase the transition rate such that the intermediate states of the transition are sufficiently populated. One solution is to drive the initial state of the lipid far from equilibrium through a rapid temperature change. Structural studies of rapid phase transition kinetics have become feasible with the advent of synchrotron radiation facilities allowing diffraction to be re-

† This work was supported by NIH Grant GM32614, DOE Grant DE-FG02-87ER60522, and ONR Grant N00014-90-J-1702. Portions of this work are also described in Tate (1987).
* To whom correspondence should be addressed.

[1] Abbreviations: L_α, lamellar phase; H_{II}, inverse hexagonal phase; SIT, silicon intensified target; DOPE, 1,2-dioleoyl-*sn*-glycero-3-phosphoethanolamine; DEPE, 1,2-dielaidoyl-*sn*-glycero-3-phosphoethanolamine; PE, phosphatidylethanolamine; PC, phosphatidylcholine; PE-Me phospho-*N*-methylethanolamine; PE-Me_2, phospho-*N*,*N*-dimethylethanolamine; T_{bh}, lamellar–hexagonal transition temperature; SCR, silicon controlled rectifier; d, basis vector length; R_w, radius of water core in H_{II} phase; $d_{H_{II}}$, minimum monolayer thickness in H_{II} phase; d_{max}, maximum monolayer thickness in H_{II} phase; a_0, area per lipid at lipid–water interface; ϕ_w, liquid-crystalline water fraction; IMI, inverted micellar intermediate.

0006-2960/92/0431-1081$03.00/0

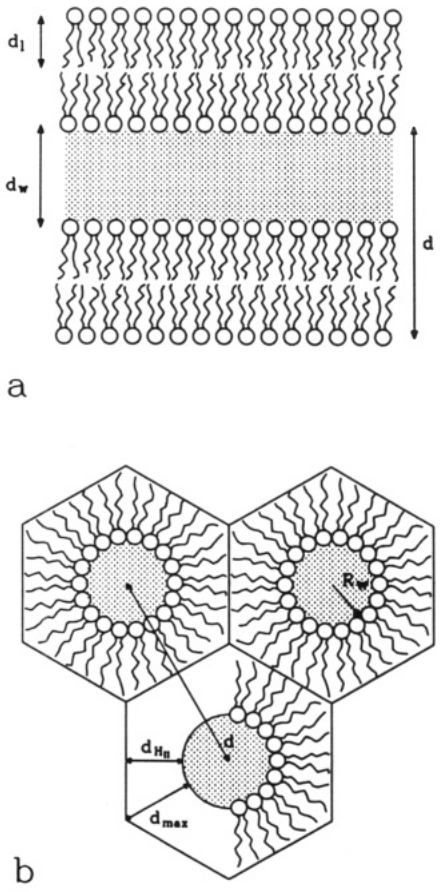

FIGURE 1: Schematic of the (a) lamellar (L_α) and (b) inverse hexagonal (H_{II}) phases in cross section. The shaded region in each figure represents water. The lamellar phase consists of alternating planar sheets of water and lipid. The H_{II} phase consists of tubes of water of radius R_w arranged on a hexagonal lattice. Each tube is surrounded by a lipid layer. d is the lattice basis vector length in each phase.

corded in times much less than 1 s [see Gruner (1987), Caffrey (1989) and Lis and Quinn (1991) for reviews]. Several groups have begun investigations into the phase transition kinetics of lipid systems (Caffrey, 1985, 1987; Caffrey et al., 1990; Cunningham et al., 1986; Quinn & Lis, 1987; Ranck et al., 1984; Laggner et al., 1987, 1989; Mencke & Caffrey, 1991). Here we present a time-resolved X-ray diffraction study of the L_α–H_{II} phase transition kinetics in phospholipid systems using an efficient two-dimensional X-ray detector at a synchrotron X-ray source. Results are also presented which show the longer time evolution behavior of the transition under small temperature changes.

Materials and Methods

Synchrotron Studies. The time-resolved X-ray diffraction data were collected at beam line X10A at the National Synchrotron Light Source (NSLS) at Brookhaven National Laboratory. This beam line, operated by Exxon Research and Engineering Co., has a platinum-coated fused silica toroidal mirror to focus the X-ray beam (Gmur & White-Depace, 1986). In addition, a double flat crystal monochromator was used to select 8.00 keV (±50 eV) X-rays from the radiation continuum. The measured X-ray intensity was 2×10^{11} X-rays s^{-1} in a focused spot size of 0.5 mm × 1.0 mm.

Diffraction patterns were collected using a silicon intensified target (SIT) area detector. This detector, built for beam line X9 at NSLS, is based on a design developed at Princeton (Milch, 1979; Gruner et al., 1982; Milch et al., 1982). The detector is operated in an integrating mode with "slow" readout of the silicon diode target. The slow readout involves presetting

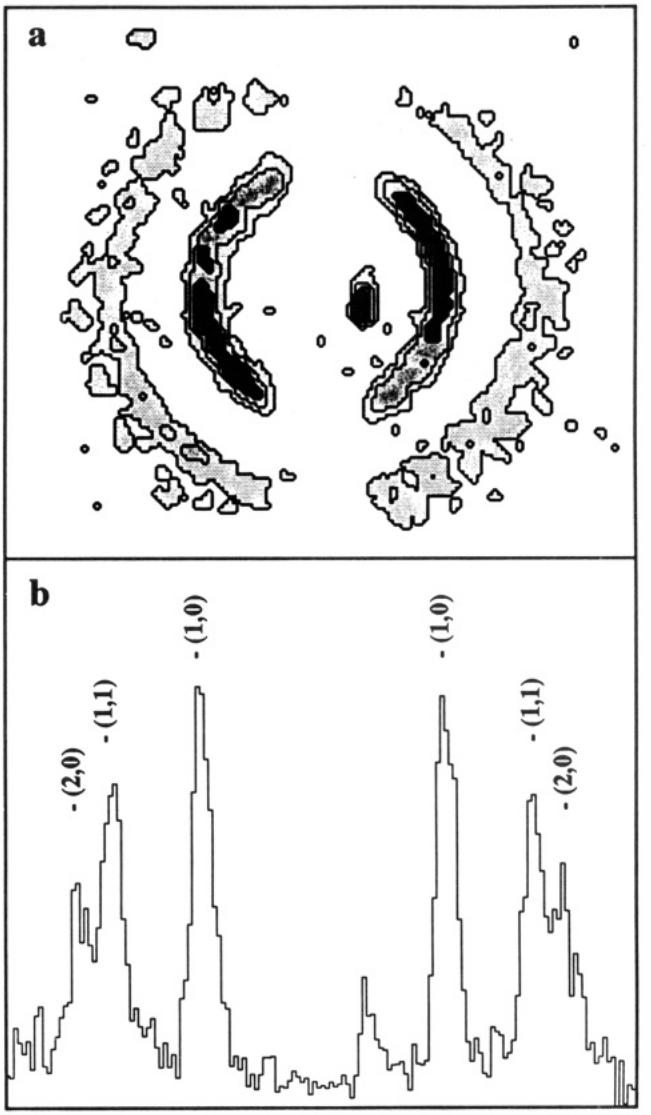

FIGURE 2: (a) Contour map of a 12-ms powder diffraction exposure from DOPE in the H_{II} phase at 15 °C. A vertical beam stop breaks each powder diffraction ring into two arcs. Some beam creep can be seen to the right of the beam stop. (b) Azimuthal integration of panel a with an angular half-width of 60° forming a one-dimensional plot of intensity vs scattering angle. Peak indices for the hexagonal lattice are indicated above each peak.

the target to a known potential, integrating the diffraction signal in analog form on the target, then digitizing the amount of charge accumulated in each of 256 × 256 picture elements (pixels). The digitized data were stored on computer disk and subsequently on magnetic tape. The entire preparation and readout procedure takes ~25 s. The narrow band-pass electronics used in the slow readout mode improve the signal-to-noise ratio and enhance the low dose characteristics of the detector at the cost of increasing the readout time for data collection. The readout time limitation necessitates repeating the data collection sequence several times, changing the window of observation each time in order to reconstruct the sequence of events. However, the data integration onto the target is a parallel process which is not limited by the instantaneous intensity of the diffraction pattern, so that very short bursts of data may be collected.

Figure 2 illustrates the capabilities of this detector at a synchrotron facility. Shown here is a 12-ms exposure from a sample of 30% DOPE (1,2-dioleoyl-*sn*-glycero-3-phosphoethanolamine) in water (w/w) at 15 °C. The (1,0), (1,1), and (2,0) peaks of a hexagonal lattice are seen. Only about 20–25

X-rays/pixel are in the most intense region of the (1,0) peak, with 4 X-rays/pixel in the (2,0) peak. The area detection capabilities of the SIT detector allow one to collect photons from the entire powder diffraction ring, improving the counting statistics compared to a one-dimensional detector. During analysis, the two-dimensional powder diffraction pattern was azimuthally integrated along an arc ±60° from the meridional (horizontal) axis to produce the one-dimensional trace in Figure 2b.

Specimens were prepared by mixing dry lipid, DOPE, or DEPE (1,2-dielaidoyl-*sn*-glycero-3-phosphoethanolamine), with 100 or 200 mM solutions of NaCl in water. This concentration of salt was chosen to make the samples electrically conductive while being low enough to have only minor effects on the phase transition temperature (Seddon et al., 1983). A 20-μL aliquot of the resulting dispersion, typically 20% lipid by weight, was placed into a electrically insulated sample cell constructed of Lucite and Teflon with thin mylar X-ray windows. Platinum foil electrodes on opposite sides of the sample allowed a pulse of current lasting 35–50 ms to be passed through the electrically conducting sample. About 1 J of energy would be dissipated within the sample through resistive heating, increasing the sample temperature by up to 35 °C. A thermoelectrically controlled copper block surrounded the inner sample cell and was used to set the "ambient" temperature of the experiment, that is, the initial temperature of the temperature jump sequence.

The DOPE was obtained from Avanti Polar Lipids within 1 month prior to the experiment and was kept at −70 °C until needed. No evidence of degradation of the DOPE was found as checked by thin layer chromatography (TLC). The DEPE stock, which was several years old, did show some degradation products. Quantitative analysis by gas chromatography and TLC showed the sample to be 95–96 mol % DEPE (analysis kindly performed by Dr. Colin Tilcock, Department of Biochemistry, University of British Columbia). The remaining fraction consisted of 1 mol % phosphatidylcholine (PC), phospho-*N*-methylethanolamine (PE-Me), or phospho-*N*,*N*-dimethylethanolamine (PE-Me_2) (PE-Me often occurring in the synthesis of PE), 1 mol % fatty acid (0.97% elaidic acid and 0.03% stearic acid), 1 mol % lysolipid (lysis of 1 mol % DEPE would account for both the fatty acid and the lysolipid), and 1–2% unaccounted for. The equilibrium phase behavior of this DEPE in excess water differed slightly from a pure DEPE sample studied at Princeton (obtained at a later time from Avanti Polar Lipids). The L_α–H_{II} phase transition temperature, T_{bh}, was lowered to 60 from 65 °C for the pure sample. The lattice spacings of the H_{II} phase at a given temperature were the same, however. The availability of DEPE was constrained by scheduling circumstances at the synchrotron. While it would have been preferable to study a pure sample, this sample can still be used in a general study of lipid systems which undergo the L_α–H_{II} transition, as long as it is recognized that the study pertains to a lipid mixture (which we hereafter refer to as the DEPE mixture), not to pure DEPE. One must look critically at the possible effects which the minor constituents within the sample could have on the kinetic behavior of the transition.

Once the sample was in place, the temperature of the copper block was set to a value typically 2 °C less than the L_α–H_{II} transition temperature, T_{bh}. After several minutes of thermal equilibration, an exposure was taken to record the initial diffraction from the L_α phase. After the readout of this exposure, the SIT target was prepared for integration. The sample was then heated internally via the pulse of current, and, at the selected time after the heating event, a fast mechanical X-ray shutter was opened to begin collection of the diffraction data of the sample in transition. The shutter consisted of a small tantalum vane attached to a lightweight aluminum arm driven by a large stepper motor (Collett, 1983). Typical exposure times were 10–300 ms. The second frame was then digitized, taking about 20 s, and then a third frame was taken. By this time the sample had cooled close to the initial temperature. The sample was then reset to the L_α phase (as monitored by X-ray diffraction), and another temperature jump was performed.

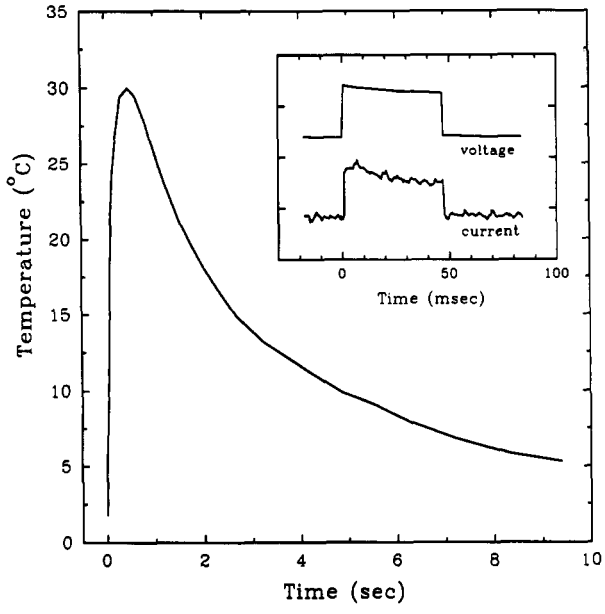

FIGURE 3: Measured thermocouple temperature as a function of time after a current pulse was passed through the sample. This thermocouple has been encased in a thin layer of glass to provide electrical insulation from the heating current. Response time is on the order of 100–200 ms. Cooling time is an order of magnitude longer. The inset shows the current through the sample and the voltage across it. Average current in this trace is 30 mA. Average voltage is ~800 V.

The current pulse through the sample was generated by discharging an 8-μF capacitor, charged to 800 V, through a silicon-controlled rectifier (SCR). After 50 ms, any remaining charge on the capacitor was shunted to ground through a second SCR. A reed relay grounded the sample completely after several additional milliseconds. The temperature of the sample was monitored with a thermocouple (Chromel–Constantan, 0.005-in. diameter) placed just above the diffracting volume. The thermocouple voltage was amplified and recorded on a digital oscilloscope (Figure 3). The thermocouple amplifier was electrically isolated for the duration of the current pulse via a reed relay on each of the thermocouple leads. Initial measurements were made with an uninsulated thermocouple with a response time of 1 ms. Since thermocouple voltages are typically in the millivolt range, grounding of the sample to better than 1 part in 10^6 was necessary within several milliseconds before the thermocouple readings could be taken. This method proved to be unreliable, so subsequent measurements were made with the thermocouple encapsulated in a thin layer of glass. This process reduced the response time of the thermocouple to about 100 ms due to thermal lag. Approximately midway through the experiment, provisions were made to monitor the sample current and voltage, providing a direct measurement of the energy dissipated within the sample. The inset to Figure 3 shows typical oscilloscope traces monitoring the energy.

The method used for heating made precise control of the temperature difficult. The magnitude of the jump depended strongly on the sample resistance. Overall resistance appeared to rely more on the condition of the platinum electrodes and on the uniformity of the lipid dispersion than on the concentration of the salt in solution. To form uniform dispersions, it was necessary to mix the lipid and buffer at a temperature corresponding to the L_α phase of the lipid. When mixed in the H_{II} phase, the lipid would form aggregates, which, when loaded into the cell, would pack so as to effectively insulate the electrodes from one another. Reproducibility was somewhat improved by performing repeated temperature jumps on the same sample.

Note that uniform heating of the entire sample volume should result in only about a 10 °C increase in temperature for every joule of energy dissipated. While 20 μL of sample was contained within the cell, only 5–10 μL of this sample was directly between the electrodes. The current would pass through this portion of the sample, heating it quickly. This volume between electrodes included both the thermocouple and the diffraction volume. This method of heating was chosen for giving large temperature jumps within a short, well-defined period of time. Studies of the temperature dependence of the transition rate would be best carried out, however, under better defined, more repeatable conditions.

Long Time Scale Studies. Longer time evolution studies of the phase transition in DOPE were carried out on a small-angle X-ray diffraction beam line at Princeton using a Rigaku RU-200 rotating anode generator to produce Cu Kα X-rays. This configuration produced ~5 × 10^7 X-rays s^{-1} in a 0.3 × 1.0 mm^2 beam. Diffraction patterns were recorded using the Princeton SIT (silicon intensified target) detector (Gruner et al., 1982). Exposure times were typically 30–200 s.

For these studies, samples were prepared by placing 5 mg of lipid in the bottom of a thin-walled glass X-ray capillary and adding 10 mg of water. After brief mechanical mixing, the capillary was sealed with epoxy. To ensure complete mixing, the sample was then subjected to several freeze–thaw cycles before data were taken. The capillary was then placed in a thermoelectrically controlled copper block contained within an evacuated chamber. By controlling the current through the thermoelectric modules, the temperature of the block may be set to temperatures between −30 and 100 °C. The temperature was stable to ±0.1 °C.

The experimental protocol involved setting the sample completely in either the L_α or H_{II} phase and then setting the temperature near the L_α–H_{II} phase transition temperature (2 °C on heating and 4 °C on cooling). After a 10-min equilibration time at this temperature, the sample temperature was then set to the target temperature (see Results), and a series of diffraction exposures was taken. Drifts in the X-ray flux were monitored with an ionization monitor placed in the beamline.

Integrated diffraction peak intensities are used as a measure of the fraction of lipid in a given phase. Integration was performed by first azimuthally integrating the two-dimensional powder-like diffraction pattern. The resulting curve of intensity vs scattering vector was then fitted to a series of Gaussian peak shapes with a quadratic background. The diffraction intensity in each phase is normalized to the intensity found when the sample is totally in the given phase. Such a measure of lipid fraction is valid only if the structure factor for diffraction changes little over the region of interest. This appears to be the case for the lamellar phase in the large temperature jumps and for both phases with smaller jumps. The structure factor for the H_{II} phase in the large temperature jumps changes rapidly with time, and hence intensity data in this case cannot be used to determine the fraction of lipid in this phase. Note that, at early times during large temperature jumps, the overlap of diffraction peaks introduces uncertainty into the determination of the lamellar peak intensities. No overlap of peaks is seen for the long time studies.

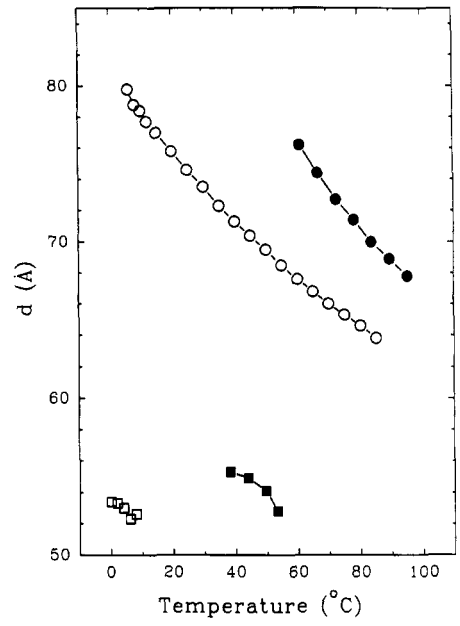

FIGURE 4: Equilibrium basis vector lengths, *d*, for DOPE (open symbols) and the DEPE mixture (closed symbols). Squares represent the L_α phase, circles the H_{II} phase. Below 40 °C, the DEPE mixture is in the L_β phase. Note the marked decrease in *d* with temperature for the H_{II} phase.

RESULTS

Equilibrium Phase Behavior. DOPE and DEPE are similar lipid species differing only in the conformation of the double bond at the ninth position within the hydrocarbon chains. The "kink" introduced by the cis double bond in DOPE reduces the L_α–H_{II} phase transition temperature, T_{bh}, from 60 °C for the DEPE mixture to ~6 °C for DOPE. At a given temperature, DOPE also has a smaller water core radius in the H_{II} phase, which is manifested in a smaller basis vector length at a given temperature. At 70 °C, the basis vector length is ~5 Å less for DOPE, 71.4 compared to 66 Å (Figure 4). Note the strong temperature dependence of *d* in the H_{II} phase resulting from progressively smaller water core radii as the temperature is increased (Tate & Gruner, 1989).

Kinetic Behavior of DOPE. Figure 5 shows a reconstructed time sequence of diffraction from DOPE undergoing the L_α–H_{II} phase transition after a large temperature jump. The data presented in this figure were obtained from multiple jumps on a single sample. The magnitude of the temperature jump in this reconstructed sequence varies from 24 to 37 °C. The diffraction from the initial L_α phase is characterized by an intense, sharp first-order Bragg diffraction peak (Figure 5a). Higher diffraction orders were seen with longer integration times. For times less than 100 ms after the temperature jump, broad and weak diffraction peaks were seen in addition to the lamellar diffraction peak, with the intensity of the lamellar peak only slightly reduced (Figure 5b). Diffraction collected after longer delays show a further reduction in the lamellar intensity with a concomitant increase in the intensity of the broad diffraction peaks seen initially (Figure

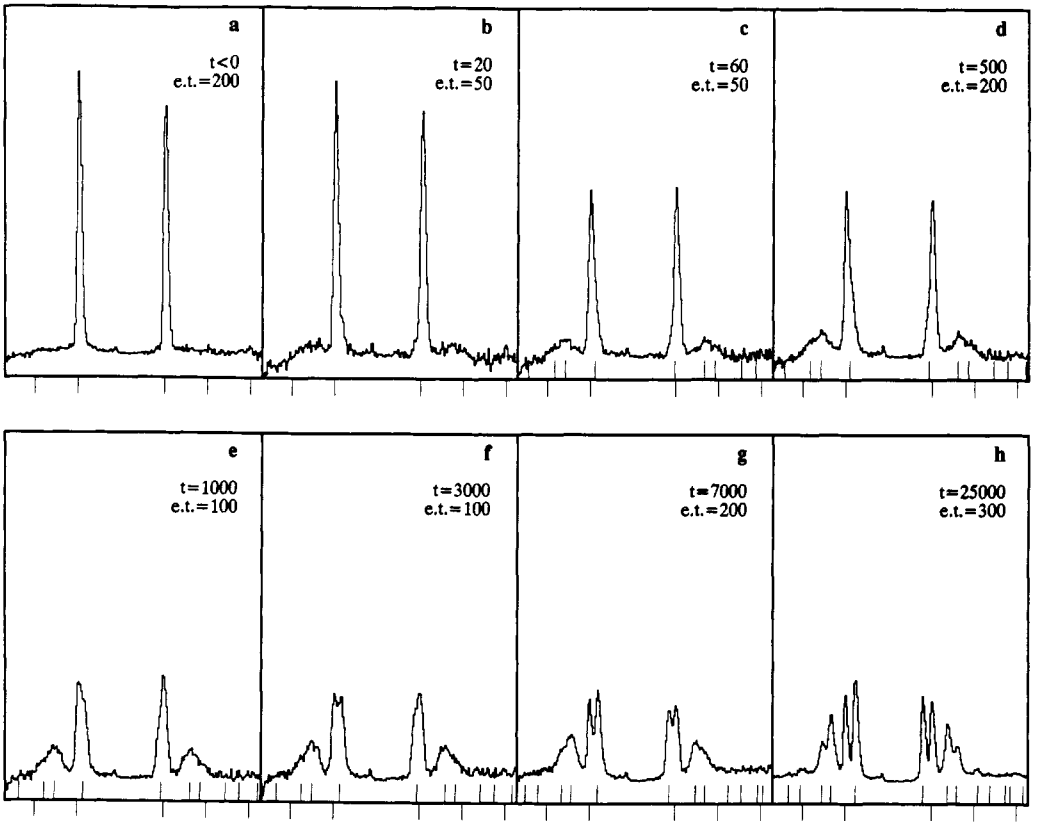

FIGURE 5: Reconstructed time sequence of diffraction from DOPE undergoing the L_α-H_{II} transition. The starting time of the exposure, *t*, relative to the heating pulse is indicated in milliseconds on each frame. The exposure time, *e.t.*, is also given in milliseconds. (a) The initial lamellar phase at 3 °C. (b) Diffraction beginning 20 ms after the beginning of the heating pulse (the pulse lasted 50 ms) and lasting for 50 ms. The lamellar diffraction has been reduced only slightly in intensity. (c–h) Reduction in the lamellar diffraction is occurring as a broad peak begins to appear. Tic marks are included under each diffraction figure to indicate the expected position of peaks from the L_α (tic marks below axis, d = 52 Å) and H_{II} phase (tic marks above axis). The spacing of the H_{II} phase at short times is assigned by assuming the peak of the broad nonlamellar diffraction corresponds to the (1,1) peak of the hexagonal lattice.

5c–h). A noticeable shoulder on the inside of the first-order L_α peak is also seen. These peaks sharpen gradually and shift in position so that by 7 s the diffraction clearly indexes to a hexagonal lattice with a small amount of residual L_α phase (Figure 5g). Note that at 7 s the peaks are still sufficiently broad so that the (2,0) peak of the hexagonal lattice is seen as a shoulder to the stronger (1,1) peak. After 25 s the peaks have sharpened such that the peak width is now limited by the width of the incident beam (Figure 5h). The (2,1) peak of the hexagonal lattice can be seen in this diffraction exposure as well as the (2,0), (1,1), and (1,0) peaks. A small amount of the L_α phase remains in this exposure as well. By this time, the temperature of the sample was no longer above T_{bh}, so that additional formation of the H_{II} phase has stopped. Diffraction collected after 52 s has changed little from that at 25 s.

Most of the jumps did not produce a complete transition to the hexagonal phase since the sample would cool sufficiently within several seconds to arrest the rapid formation of the hexagonal phase (Figure 3). If the temperature was kept high using multiple current pulses through the sample, complete formation of the hexagonal phase was seen. Although the sample had cooled to below T_{bh} by 30 s, the diffraction from the DOPE sample was seen to be stable for several minutes at this temperature, with the relative intensities of the diffraction from each phase as well as the lattice size of each phase remaining constant. Due to this stability, the third diffraction exposure in the temperature jump sequence can therefore be used a measure of the completeness of the transition. The stability of the diffraction at this temperature also shows that the reverse transition from H_{II} to L_α is very slow for small temperature changes. In fact, to reset the DOPE sample into the L_α phase for subsequent jumps within a reasonable amount of time, the lipid needed to be cooled into the L_β phase (<−10 °C) and then warmed into the L_α phase.

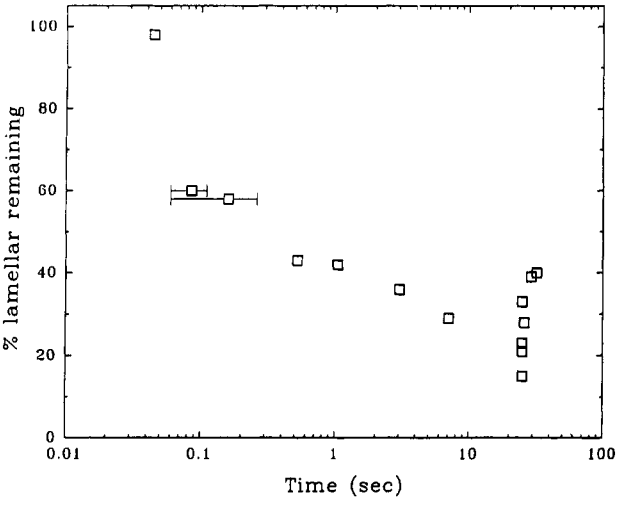

FIGURE 6: Fraction of the lamellar phase remaining for the temperature jumps represented in Figure 5. The lamellar fraction was measured using the intensity of the first-order peak. The percentages measured at 25 s and beyond are seen to be stable over the course of several minutes as the sample has cooled just below the transition temperature. Error bars are used to indicate the time window during which the diffraction was collected.

Figure 6 shows the fraction of the lamellar phase remaining as a function of time for the series of temperature jumps depicted in Figure 5. The intensity of the lamellar diffraction peak was reduced approximately by 50% within 150 ms. The

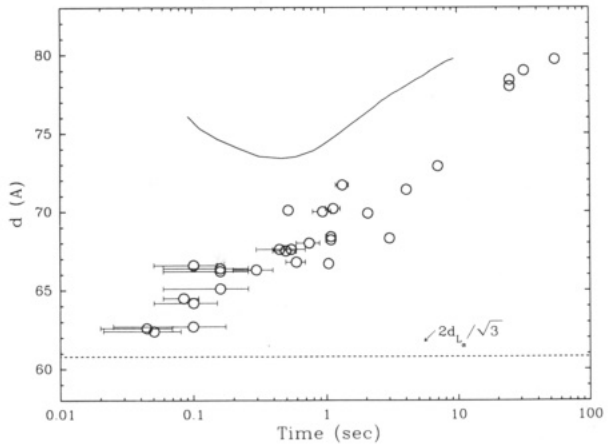

FIGURE 7: Hexagonal basis vector length, d, for DOPE as a function of time after the heating event. Points are obtained from temperature jumps with a wide variety of peak temperatures and a large variation in the fraction of H_{II} phase present. The solid curve represents the equilibrium spacings of an H_{II} lattice at the temperature measured by the thermocouple. This curve was obtained from a representative thermocouple trace in the series of jumps with the highest temperature change (~30 °C) (see Figures 3 and 4). The dashed line indicates the H_{II} spacing which would be commensurate with the initial L_α phase ($d = 2d_{L_\alpha}/\sqrt{3}$). The error in the determination of the basis vector length is ±3 Å at times less than 300 ms. At 7 s, this is reduced to ±1 Å, and at 25 s, ±0.5 Å.

diffraction recorded during the third exposure in each of these temperature-jump sequences shows a variation from 16 to 40% in the amount of the L_α phase remaining. No correlation was found, however, between the temperature recorded by the thermocouple and the fraction of the sample remaining in the L_α phase after 25 s. Little correlation for this series was seen between the final L_α fraction and the number of cycles that the sample has undergone, although the temperature change as measured by the thermocouple was greater for each successive jump.

There are several factors which could account for the broadness of the nonlamellar diffraction peaks during the early portions of the temperature jump. If the liquid-crystalline domains are of limited size, then the line shape of the peaks would be characteristically broadened. Alternatively, different nonlamellar domains throughout the sample could have different lattice constants or there could be lattice disorder within the growing domains (Guinier, 1963). No direct evidence was seen for any intermediate structures forming during the time scale of the experiment other than the H_{II} tubes themselves. Diffuse scatter from intermediate structures which are not packed on a lattice would be difficult to distinguish above the broad H_{II} diffraction peaks, even at concentrations up to several percent. To see evidence of intermediate structures in such quantities would require that they be packed in a lattice, giving rise to sharp diffraction peaks.

Attempts to reconstruct a time sequence of diffraction from data collected from different samples proved difficult due to variability in temperature jumps between samples. One feature of the nonlamellar diffraction was remarkably consistent in spite of this large variability. Figure 7 shows the H_{II} lattice spacing, d, as a function of time after the heating pulse. These spacings are seen to increase monotonically with time, approaching 80 Å, the equilibrium value of d for DOPE at 6 °C. Note that this figure includes data from both large and small temperature jumps. There is little correlation between the fraction of the sample remaining in the L_α phase and time, due to the variability in the magnitude of the jumps.

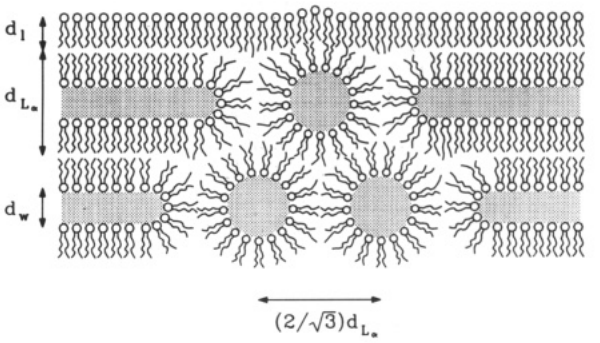

FIGURE 8: Commensurate L_α and H_{II} lattice. Rapid formation of a commensurate H_{II} lattice within a lamellar structure could occur without bulk transport of lipid or water, leaving the H_{II} lattice in a highly stressed state. Additional water would be brought into the lattice as the H_{II} phase swells to its equilibrium value.

From Figure 4 we see that d in the H_{II} phase for a sample in thermal equilibrium depends strongly on temperature. Recall that the sample is cooling after the initial heating pulse. A sample in thermal equilibrium throughout the temperature-jump sequence would exhibit a monotonic rise in d as a function of time. However, the H_{II} spacings measured in the kinetic diffraction are much less than d for a sample in thermal equilibrium, even when compared to the largest temperature changes recorded (Figure 7). Here the measured spacings are up to 10 Å less than the corresponding equilibrium values. After ~30 s, the equilibrium and measured values of the spacing begin to coincide.

There is no reason to expect that the H_{II} lattice should be in equilibrium as the transition proceeds. After formation of a H_{II} tube, the lipid and water undergo a rearrangement as the H_{II} lattice swells to the equilibrium spacing. Note that the equilibrium H_{II} lattice has seven additional water molecules per lipid as compared to the L_α phase (Gawrisch et al., 1990), thus bulk transport of material must take place. The initial size of the H_{II} lattice is very close to a value commensurate with the L_α lattice. For this reason, the (1,0) peak of the hexagonal lattice was masked by the lamellar peak. If the H_{II} phase is formed in a commensurate transition, then with certain types of mechanisms, little bulk transport of either lipid or water would be necessary for the initial formation of the tubes [Figure 8; see also Gruner et al. (1985)]. Assuming that the H_{II} tubes form with no bulk transport of material, then the local water concentration, ϕ_w, will be the same for both phases. These assumptions allow us to calculate the internal dimensions of the initial H_{II} phase (Figure 1b). The water core has a radius R_w = 16.2 Å, and the lipid takes on lengths from $d_{H_{II}}$ = 13.8 Å to d_{max} = 18.4 Å. The area of a lipid molecule at the water interface, a_0, is 54 Å^2. These calculations use d = 52 Å for the lamellar phase (Gruner et al., 1988) with 11 water molecules per lipid (Gawrisch et al., 1990). These internal dimensions indicate that the H_{II} phase is in a highly stressed state. Compare to the equilibrium values of DOPE at 20 °C: R_w = 21.6 Å, $d_{H_{II}}$ = 16.2 Å, d_{max} = 22.0 Å, and a_0 = 47.4 Å^2 (Tate & Gruner, 1989). The relatively slow process of rearrangement of the water and lipid into the larger H_{II} lattice probably limits the swelling of the lattice once it is formed. The water tubes of the H_{II} phase are likely to have no direct connection with each other or with the bulk phase, since H_{II} tubes truncated directly into the bulk water would expose the hydrocarbon region to the water, increasing the free energy of the system. Consequently, the movement of water is likely to be highly impeded.

Kinetic Behavior of the DEPE Mixture. Kinetic diffraction experiments were also performed on the similar lipid species

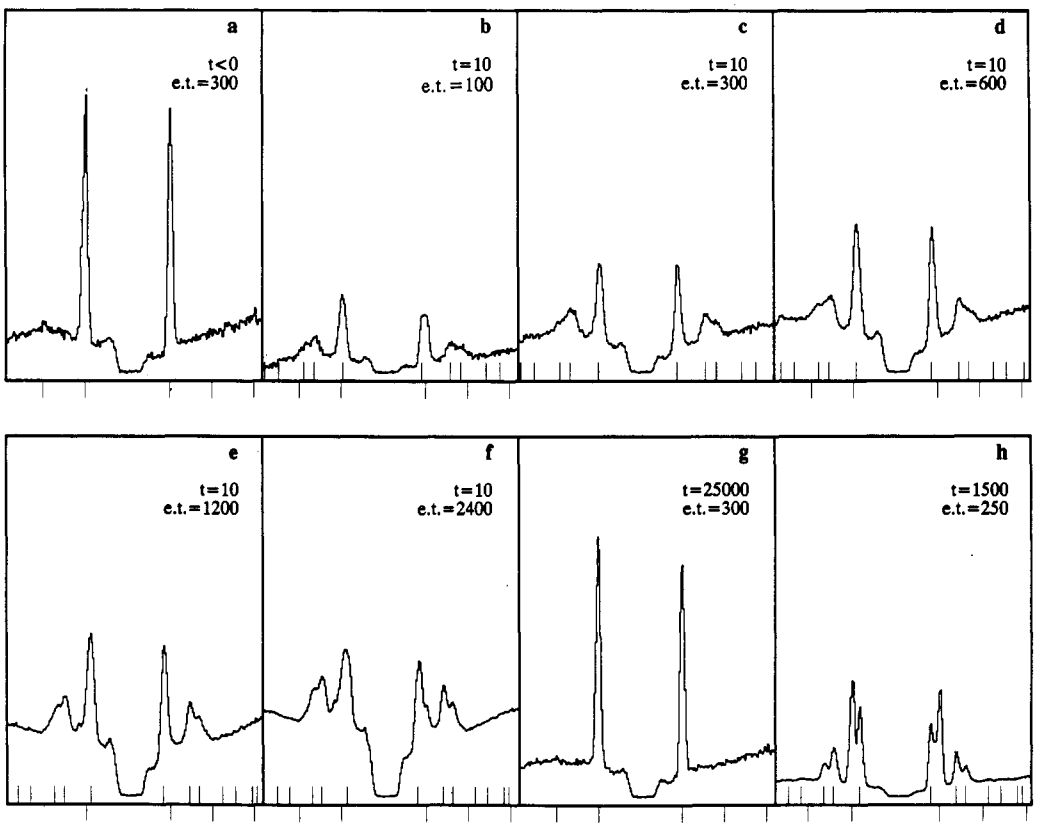

FIGURE 9: Reconstruction of the time sequence of diffraction from a DEPE mixture undergoing a temperature jump. See Figure 5 for an explanation of symbols. The initial L_α phase is shown in panel a. Note that the transition occurs much more quickly than for DOPE. Also, the system has returned to the L_α phase by 25 s. Exposures d–f were taken with large windows of time. The expansion of the H_{II} lattice with time contributes to the broadness of the diffraction peaks in these frames. Diffraction from a sample undergoing a smaller temperature jump is shown in panel h. The widths of the peaks in this narrow time slice are limited by the thickness of the incident X-ray beam. Tic marks show expected peak positions of the L_α (tic marks under axis) and H_{II} lattice. Lamellar tics shown in panels b–f assume that the L_α phase has the same spacing (d = 54 Å) as in panel a.

DEPE in the presence of trace contaminants (see Methods). A reconstruction of the diffraction as a function of time is shown in Figure 9. Again the H_{II} peaks were initially broad and seen to sharpen with time. The kinetic behavior of the DEPE mixture was distinctly different in several respects. First, the time required for the sample to undergo the L_α–H_{II} transition was much less. Figure 9b shows that, in the time window from 10 to 110 ms after the start of the heating pulse, the L_α diffraction peak has been reduced in intensity by at least 75%. This reduction in intensity has been *underestimated* since L_α and H_{II} peaks are superimposed at this time. The diffraction in Figure 9b was associated with an 18 °C jump in temperature, with 0.8 J having been dissipated in the sample. A jump dissipating 0.4 J into the sample also showed that a similar fraction of the sample had undergone the transition into the H_{II} phase during this same time period. Second, the transition back into the L_α phase from the H_{II} phase was seen to be rapid. The diffraction collected during the third exposure of a temperature jump sequence (25 s after the heating pulse) showed that most of the sample has returned to the L_α phase (Figure 9g). The temperature of the sample at this time was only 1–2 °C less than T_{bh}. The corresponding return to the L_α phase for DOPE took longer than 10 min. Third, the diffraction from the H_{II} lattice is seen to sharpen much more quickly for the DEPE mixture, as the (2,0) peak is beginning to be seen by 1 s (Figure 9e). Note that the diffraction in Figure 9d–f was unfortunately taken with long windows of time, so that the width of the diffraction peaks may be due to the size of the lattice changing over this period of time. Figure 9h shows diffraction taken 1.5 s after a small temperature jump using a 100-ms time window. The peak widths are here limited by the size of the beam.

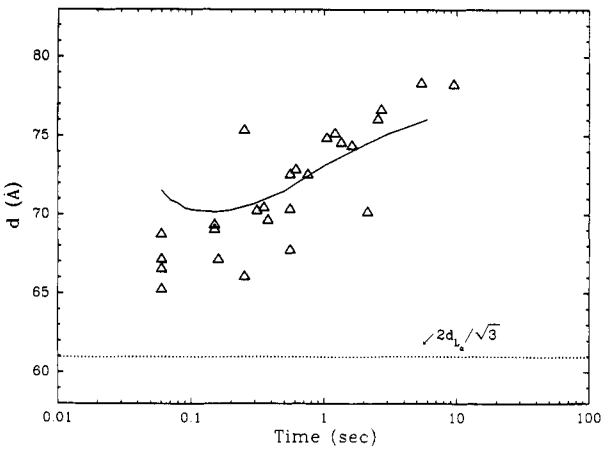

FIGURE 10: H_{II} basis vector lengths for a DEPE mixture as a function of time after the temperature-jump heating event. The solid curve represents the basis vector lengths expected from a DEPE sample in thermal equilibrium at the temperature indicated by the thermocouple for a 30 °C temperature jump. Note that this curve agrees much more closely with the measured value of d than in the DOPE case (Figure 7). The dashed line indicates the H_{II} spacing which would be commensurate with the initial L_α lattice.

The spacings of the H_{II} domains during transition are seen to increase with time, again swelling from a lattice commensurate with the L_α phase (Figure 10). The lattice swelling is seen to occur at approximately the same rate as for DOPE. However, if one compares the equilibrium spacings of the H_{II} lattice in the DEPE mixture, even for moderate temperature changes, they are seen to agree much more closely with the

Table I: Time Constants for L_α–H_{II} Phase Transition as a Function of Final Temperature[a]

	temp (°C)						
	heating				cooling		
	4	6	8	20	0	−2	−5
x	1	0.07 ± 0.01	0	0	0	0	0
t_0 (s)	20210 ± 400	7950 ± 3000	–	–	–	–	–
t_1 (s)	–	501 ± 20	98 ± 3	<20	918 ± 40	80 ± 6	9 ± 5
t_2 (s)	–	97 ± 6	46 ± 2	–	22 ± 3	70 ± 4	56 ± 14

[a] Heating values are from an initial L_α phase at 2 °C. Cooling values are from an initial H_{II} phase at 4 °C. The fitted function is of the form

$$y = x[1 + (t - t_2)/t_0]^{-1/2} + (1 - x)e^{-(t-t_2)/t_1}$$

where y is the fraction of the initial phase remaining at t, time and x characterizes the fraction of the decay occurrng via an algebraic process. t_2 is introduced as a thermal lag time for the system. A "–" symbol indicates the parameter was excluded from the fit. The fitted functions are shown in Figures 11 and 12.

measured kinetic spacings. These values are much closer to the commensurate spacing than for DOPE. Since the H_{II} spacing for the DEPE mixture is lower than DOPE at their respective values of T_{bh}, each having similar L_α spacings, commensurate structures with a value of curvature much closer to equilibrium can be formed with the DEPE system. The transitory intermediates will be at a lower free energy, creating less of a barrier to the transition for the DEPE mixture.

The question of the purity of the DEPE should be addressed since the sample did contain about 1 mol % fatty acid and lysolipid. Although the equilibrium lattice dimensions in the H_{II} phase agreed closely with pure DEPE, T_{bh} was lowered by 5 °C. It was observed that if the DEPE sample was not reset to the L_β phase after each jump, then over the course of eight or more consecutive jumps, diffuse diffraction was seen in addition to the lamellar peaks. After 20 cycles through the L_α–H_{II} transition, very little of the sample remains in the L_α phase. The sample could be returned to the L_α phase only by first cooling into the L_β phase at 25 °C and then reheating. This is similar to behavior observed for DOPE-Me (Gruner et al., 1988). Many more cycles in temperature were necessary before similar behavior was seen in pure DOPE (Shyamsunder et al., 1988). Further temperature cycling in the pure DEPE, as well as DOPE, resulted in diffraction from a well-ordered cubic lattice. It is not unreasonable to expect that the fatty acid and lysolipid impurities in the DEPE sample could have a profound effect on the rate of the L_α–H_{II} transition. Monomer solubilities of lysolipids in water are much higher than their diacyl counterparts. This could potentially reduce the activation barrier between states, thereby increasing the transition rate.

Small Temperature Jump Behavior. The slow time evolution of the L_α–H_{II} phase transition in DOPE for small temperature jumps was also studied at a rotating anode X-ray source (see Materials and Methods). Shown in Figure 11 is the decay in the intensity of the first-order lamellar diffraction peak for samples set to one of several final temperatures. Each sample began entirely in the lamellar phase at 2 °C. Fitted time constants for the decay are given in Table I. Concomitant with the reduction in the lamellar intensity is a rise in the fraction of the sample in the H_{II} phase (data not shown). The lamellar plus H_{II} fractions over the course of the experiment was found to be unity within experimental error. At 4 °C, the sample is slowly evolving into the H_{II} phase over the course of a week, at which time 15% of the sample was still in the lamellar phase. This long time evolution can be fit well by a power law of the form $(1 + t/t_0)^{-1/2}$, where the decay time t_0 is 2.0×10^4 s. Note this fit covers over four decades in time (Figure 11).

When the sample is heated from 2 to 6 °C, the time dependence of the lamellar peak intensity can be separated into

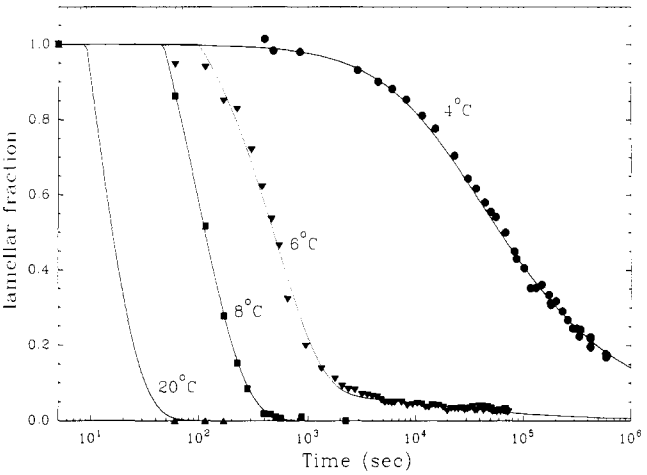

FIGURE 11: Long time kinetics of the L_α–H_{II} phase transition for small temperature jumps. Shown is the fraction of lamellar phase remaining as a function of time after heating a DOPE sample from 2 to 4, 6, 8, and 20 °C. The solid curves are fits to power law and exponential decay functions. See Table I for fitted parameters. The 4 °C data follow a power law decay over four decades in time, with 15% of the sample remaining in the L_α phase after a week.

three regions. After a period of roughly 100 s, in which the lamellar intensity decreases only slightly, the lamellar peak intensity begins to fall exponentially with a time constant of about 500 s. At about 1000 s, the conversion of the sample into the hexagonal phase reverts to a power law behavior. The initial period of inactivity may be explained, at least in part, by thermal lag within the system. Zero time indicates when the temperature change was initiated. Tests with a thermocouple within a glass capillary show a roughly 40-s lag time for a 5 °C change in temperature. The solid line fit to the 6 °C data in Figure 11 is a function of the form

$$y = x[1 + (t - t_2)/t_0]^{-1/2} + (1 - x)e^{-(t-t_2)/t_1}$$

where y is the fraction of lamellar phase remaining after time t, t_0 is the time constant for the power law decay, t_1 is the time constant for exponential decay, and t_2 is a time to characterize the thermal lag in the system. The parameter x specifies the relative weights between the exponential and power law decay. Note that the 4 °C data described above also fit this function using a weight of $x = 1$.

The thermal lag in the system is again seen when heating to 8 °C. The time constant for the exponential decay in the lamellar intensity is much shorter now, roughly 100 s. Furthermore, no long time power law behavior is seen at this temperature. Heating to 20 °C further increases the transition rate, as the sample converts from completely lamellar to completely H_{II} in the 25-s readout interval between the first and second exposures of the sequence. Similar behavior in

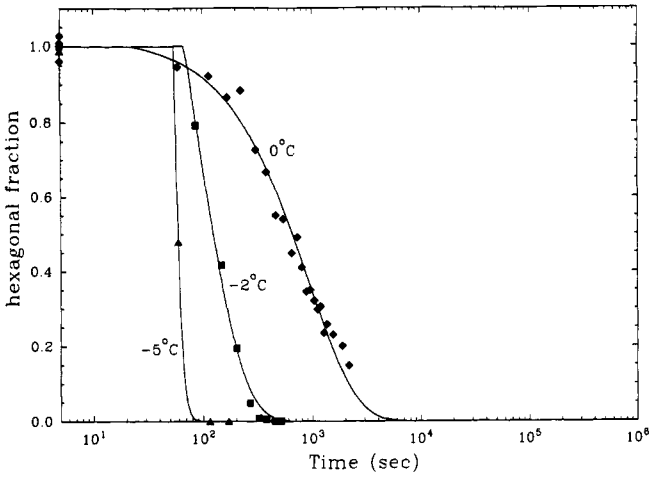

FIGURE 12: Fraction of H_{II} phase remaining in DOPE after cooling from 4 to 0, −2, and −5 °C. Each curve is fit to a exponential decay function with an included offset for thermal lag in the system (see Table I).

the time evolution was observed on cooling from the H_{II} to L_α phase (Figure 12). The decay of the hexagonal peak intensity at 0 and −2 °C roughly parallel the decay of the lamellar intensities observed at 6 and 8 °C, respectively, indicating that the true equilibrium transition temperature should be near 3 °C.

Note that, in this series of experiments, once thermal uniformity is achieved, the lattice spacings for both the L_α and H_{II} phases do not change with time, only the relative intensities of the peaks as the sample converts from one phase to the other. This implies that the lipid and water are free to rearrange within a given mesophase into the equilibrium structure at a much faster rate than the phase conversion. This should be expected in light of the results from the rapid kinetic studies performed at the synchrotron. There it was found that the swelling times for the H_{II} phase were on the order of 20 s, much faster than the time scale for the phase transition for these small temperature jumps. Also note that the lattice size of the H_{II} phase, which has a strong temperature dependence, always rapidly achieved the value expected for the temperature of the sample. This indicated that the sample was thermally homogeneous at the expected temperature within about a minute. Thus the slow conversion of the L_α phase to the H_{II} phase could not have been due to thermal inhomogeneities.

Discussion

The lipid layers in the L_α and H_{II} phases have different topologies. The lamellae must be torn, exposing some of the hydrocarbon region to water, in order to form the H_{II} phase. This momentary exposure is likely to produce a large barrier to the kinetics of the transition. A successful kinetic model of the transition should provide a mechanism for the rearrangement of the lipid and water. In the following discussion, the mechanisms presented are rough ideas based on the little experimental evidence available. Calculations of transition rates via such intermediates are still in the early stages.

There have been several proposals for the structures mediating the L_α-H_{II} transition. Using freeze fracture electron microscopy (EM), micellar structures ("lipidic particles") have been seen in some H_{II} forming systems near T_{bh} (Verkleij et al., 1980; Verkleij, 1984). In certain photographs, these micelles are collinear with an adjacent H_{II} phase, suggesting that the H_{II} tubes have formed from a coalescence of the micelles. Such photographs have led to a number of papers proposing inverted micellar intermediates mediating the morphological change from L_α to H_{II} as well as the change necessary to fuse two cells (Verkleij, 1984; Cullis et al., 1985). EM of other H_{II}-forming systems, such as DOPE, show little indication of "lipidic particles".

Siegel (1984) calculates that one type of intermediate structure, inverted micellar intermediates (IMI's), should form between bilayers quickly at temperatures near or above T_{bh}. Large fluctuations in the lipid concentration would not be necessary for these structures to form, although two monolayers would have to come into close apposition, increasing the hydration free energy of the system. The coalescence of the IMI's into linear H_{II} tubes would, however, take much longer than the transition times observed for many systems (D. Siegel, personal communication). In addition, this type of mechanism would not explain the length of H_{II} tubes observed in EM ($\sim$10 μm). Also, the lifetime of the IMI's which Siegel calculates would be much too short to be seen with conventional EM techniques. The lipidic particles seen in EM are likely to be different than the IMI. The micellar structures that have typically been seen by EM are usually systems which also are seen to have an isotropic NMR signal, thus these "lipidic particles" may be structures leading to formation of one of the several cubic phases (Gruner et al., 1988).

There are other proposed intermediate structures which form between adjacent bilayers undergoing a transition to a nonlamellar phase (Siegel, 1986a–c, 1987). Using the specialized technique of time-resolved cryotransmission electron microscopy, Siegel and co-workers have imaged isolated intermediate structures in vesicular systems undergoing a transition to the hexagonal phase (Siegel et al., 1989). Such techniques promise to shed even more light on the topological changes that accompany these phase transitions.

To explain the length of the H_{II} tubes, cooperative mechanisms have been proposed (Caffrey, 1985; Hui et al., 1983). After formation of one tube, the surrounding bilayers are perturbed, causing ripples to be formed within the bilayer, thereby causing adjacent bilayers to be in close apposition along lines parallel to the initial tube. The bilayers coalesce at these points, forming additional H_{II} tubes. Note that such a mechanism will allow long H_{II} tubes to form quickly. One may argue that the hydration repulsion force acting over such a large area, as well as the necessity of exposing a great deal of hydrocarbon to water, would disfavor this type of mechanism. The formation of small defects, such as the IMI's would be expected to have much less of an activation energy barrier. A highly cooperative transition may overcome these limitations, however.

Siegel (1986a–c, 1987) has proposed that the IMI structures may seed line defects as an alternative to their coalescing into the tubes directly. These defects would initially be small but could lengthen quickly ($\sim$cm s^{-1}). As the lipid is drawn into the defect, adjacent defects would be drawn together, forming long H_{II} bundles. The cooperative transition mentioned above could also proceed due to a propagation of a line defect, the defect essentially zipping the bilayers together (Hui et al., 1983).

Note that each of these models involves structures forming between two bilayers. Thus, each of these mechanisms can form H_{II} tubes commensurate with the L_α lattice. H_{II} tubes forming from single layers, such as fluctuations within the bilayer causing a tube to be pinched off (Borovjagin et al., 1982), are likely to not be commensurate. None of the mechanisms proposed imposes the condition that the local water concentration, ϕ_w, be constant during the transition, although none excludes it either. Note that the X-ray dif-

fraction data taken here are of insufficient resolution to determine ϕ_w directly. Of the models proposed, the cooperative transition is the most likely to keep ϕ_w constant. This would be the case if the H_{II} tubes form more quickly than bulk quantities of lipid or water could be moved. The other mechanisms rely on the movement of lipid and water for the formation of the H_{II} tubes.

The relatively long time for the swelling to occur suggests that mass transport within the H_{II} domains is limited. Transition mechanisms which involve diffusion of the intermediates, such as the aggregation of inverted micelles, or line defects being brought together, may be disfavored. The diffusion of these structures is occurring along a monolayer, however. Diffusion of lipid within a monolayer has been shown to be rapid (Small, 1986). Once the H_{II} tubes form, however, lipid transport will be between monolayers. Rates for lipids to flip from one side of a monolayer to the other are extremely slow and are measured to occur on the order of days (Small, 1986).

The lamellar lattice surrounding the H_{II} domains, by resisting elastic deformations, may also limit the swelling of the H_{II} tubes. While the lamellar lattice determines the initial size of the H_{II} tubes, the L_α lattice is not expected to be the major limitation to the swelling since DOPE samples were seen to be largely in the H_{II} phase with dimensions still very much below the equilibrium values. Also there is no correlation between the H_{II} lattice dimension and the fraction of the lipid in the H_{II} phase (the fraction varied widely in the data presented in Figure 7).

Other groups have investigated the kinetics of the L_α–H_{II} transition using various methods to initiate the transition. Caffrey and co-workers have used several heating techniques, including flowing hot air around the sample as well as microwave heating (Caffrey, 1985; Caffrey et al., 1990; Mencke & Caffrey, 1991). These techniques resulted in heating rates on the order of 30 °C s^{-1}, slower than those reported here. Transition times for dihexadecyl-PE were found to be <3 s. The initial H_{II} peaks were seen to be only slightly broadened in width, with the H_{II} lattice forming at a spacing well above a commensurate spacing for the lamellar phase. The heating rates in this case are probably not high enough to sufficiently populate a H_{II} lattice with the reduced spacing. Laggner et al. (1989) have investigated the L_α–H_{II} phase transition in 1-stearoyl-2-oleoyl-PE with a much quicker laser-induced temperature jump. They achieved 10 °C jumps in the millisecond time range. A rapid thinning of the lamellar lattice to 51 Å was seen initially, followed by the formation of the H_{II} lattice with a spacing of 68 Å beginning at 30 ms. This lattice then was seen to swell to a final value of 73 Å. All diffraction peaks were sharp throughout the phase transition. In contrast, our experiments give no indication of the initial thinning of the lamellar phase nor did we see such a large discontinuity in the lamellar and H_{II} spacings on short time scales. Differences in heating method, heating rate, lipid used, or in the magnitude of the temperature jump may account for these differences.

In simple kinetic models of a phase transition, the free energy difference between the two phases drives the transition, with the intermediate structures in the transition process, being at a higher free energy, presenting a rate-limiting activation barrier. Such models predict the conversion from one phase to the other to occur exponentially, with the exponential time constant depending on the height of the barrier and the free energy difference between the phases (which depends on how far the temperature is pushed into the second phase region). For large temperature jumps (>5 °C) into the H_{II} phase region, the data are indeed consistent with exponential kinetics. By contrast, small temperature jumps barely into the H_{II} region result in very slow conversion of the sample to the H_{II} phase. This is not a simple case of a long exponential time constant due to the small free energy difference between the two phases. The conversion in this case follows $1/\sqrt{\text{time}}$ kinetics, and, at 4 °C, the conversion of DOPE from the L_α to the H_{II} phase is still proceeding after a week! Mechanisms producing such conversion kinetics are not readily apparent, considerably complicating the discussion of the pathway(s) of the phase transition.

The algebraic time dependence of the transition under small temperature steps has both important experimental and theoretical implications. The change in symmetry between the L_α and H_{II} phases strongly suggests that the transition should be first order. If so, one expects that, for sufficiently slow scan rates, the transition enthalpy peaks determined calorimetrically should sharpen arbitrarily for excess water samples. It has always been puzzling that even at scan rates of a few degrees per hour, the L_α–H_{II} transition enthalpy peak is broad. Moreover, scan rates as low as a few degrees per hour show different transition temperatures depending on whether one is cooling or heating.

The calorimetric data are not so puzzling in view of the presence of algebraic kinetics: the transition will not have gone to practical completion even at scan rates of several degrees per week! Our observations suggest that the true transition temperature should be determined not by scanning more slowly but by careful comparison of the rates of conversion to the H_{II} phase as a function of the final temperature for small temperature steps. Presumably, once the true conversion temperature is reached, no H_{II} phase will be apparent, even after extended periods of time. Perhaps this temperature can be determined by extrapolation of the time constants of the algebraic fits to progressively smaller temperature steps. It would be of interest to see if the transition temperature defined in this way is less dependent upon whether the transition is done upon heating or cooling. Note that this also suggests that a probe sensitive to the mass fraction of the phases present, such as X-ray diffraction or NMR, may yield more accurate transition temperatures than practically performable calorimetry. One could possibly take the average of heating and cooling transition temperatures determined with conventional methods if it can be shown that the transition kinetics are symmetric with respect to the direction of the transition. For DOPE, the transition kinetics do appear to be symmetric about 3 °C. This averaging method would not be applicable to the case of limited water samples, where equilibrium coexistence of the liquid-crystalline phases is allowable. Note that almost all the statements in this paragraph run counter to the conventional wisdom with respect to lipid phase transitions.

We speculate that the peculiar nature of the L_α–H_{II} phase transition is a consequence of the necessity of disrupting the integrity of the lipid–water interface during the transition. Such a disruption probably incurs a large local free energy cost which acts as a barrier to the transition. However, the effective height of the energy barrier may well be a function of the volume concentration of such disruptive events per unit time. Taken together with the larger free energy difference between the phases, large numbers of such "rips" in the lipid–water interfaces may be responsible for the rapid conversion process seen with large temperature jumps. Additionally, if the introduction of lipid–water interface disrupting events is important to the rate of transition, then the net transition rate

is likely to be highly sensitive to the presence of lattice defects [see also Shyamsunder et al. (1988)]. Initial optical observations of lamellar specimens having macroscopically large domains suggest that the H_{II} phase first appears near defects (L. Zeger and S. Gruner, unpublished observations). If confirmed, this would add yet another complication to understanding topologically discontinuous mesomorphic transitions.

Concluding Remarks. Rapid formation of the H_{II} phase within a lamellar lattice in our experiments appears to occur via a commensurate mechanism. The H_{II} lattice then swells over the course of the next few seconds to its equilibrium spacing. Kinetic barriers limiting the rate of transition come from several sources. There is the high cost of exposing the hydrocarbon region of the lipid to water as the topology of the interface changes. Secondly, the initial H_{II} structures are not necessarily in the most energetically favorable form. Bulk transport of water into or out of the system will, in general, be necessary as the transition proceeds and the system comes into equilibrium. The relative quickness of the phase transition in the DEPE mixture compared in DOPE may involve a reduction in both of these barriers; the equilibrium spacing of the H_{II} phase in the DEPE mixture is closer to commensurate to the lamellar phase than DOPE, and the increased solubility of the lysolipid monomers in water should reduce the energetic cost of forming the H_{II} phase.

Many more experiments are necessary to sort out the important factors of the transition. The diversity of lipids forming the H_{II} phase allows many parameters to be varied. The transition temperature can be varied, as can the commensurability of the equilibrium lattices or the ratio of ϕ_w in the equilibrium L_α and H_{II} phases. Addition of small quantities of alkanes may determine if some transitions are limited by the interstitial packing requirements of the intermediate structures.

Kinetics of the transition are also likely affected by the presence of defects and domain boundaries within the sample. Line defects, for instance, are likely places to seed the growth of an H_{II} domain. Study of these effects requires the preparation of samples in which the defect density is well characterized. The possible dependence upon the defect density and the problems associated with algebraic transition rates emphasizes the need for attention to the way specimens are prepared and phase transitions are probed.

Further refinements of the experimental methods would help to better characterize the transition. Foremost would be an improvement in the method to induce the phase transition. Changes in hydrostatic pressure can also induce the phase transition and offers a well-controlled mechanism for changing the environment of the lipid in a rapid yet uniform way. The use of thin oriented lipid films would allow rapid temperature changes while increasing the intensity of the diffraction peaks, thereby improving the possible time resolution of the experiment. The initial L_α diffraction in this case would lie along one axis, allowing the diffraction from structures along the lamellar axis to be compared with that occurring off axis.

Finally, the transition between L_α and H_{II} is but one of a number of topology changing phase transitions in lipid systems. The kinetics into cubic phases can be even more hysteretic than the transitions described in this work (Gruner et al., 1988; Shyamsunder et al., 1988; Siegel & Banschbach, 1990). These and other transitions need to be studied with a variety of probes if mechanisms for lipid bilayer disruption are to be understood.

ACKNOWLEDGMENTS

We thank Colin Tilcock for his assistance with the chromatography, Dave Turner for help with the data acquisition, and Dave Siegel for profitable discussions.

Registry No. DOPE, 4004-05-1; DEPE, 19805-18-6.

REFERENCES

Borovjagin, V. L., Vegara, J. A., & McIntosh, T. J. (1982) *J. Membr. Biol. 69*, 199–212.
Caffrey, M. (1985) *Biochemistry 24*, 4826–4844.
Caffrey, M. (1987) *Biochemistry 26*, 6349–6363.
Caffrey, M. (1989) *Annu. Rev. Biophys. Biophys. Chem. 18*, 159–186.
Caffrey, M., Magin, R. L., Hummel, B., & Zhang, J. (1990) *Biophys. J. 58*, 21–29.
Collett, B. (1983) *The Passive Mechanics of Muscle: A Preliminary Structural Study*, Ph.D. Thesis, Princeton University, Princeton, NJ.
Cullis, P. R., Hope, M. J., de Kruijff, B., Verkleij, A. J., & Tilcock, C. P. S. (1985) in *Phospholipids and Cellular Regulations* (Kuo, J. F., Ed.) pp 1–59, Vol. I, CRC Press, Boca Raton, FL.
Cunningham, B. A., Lis, L. J., & Quinn, P. J. (1986) *Mol. Cryst. Liq. Cryst. 141*, 361–367.
Ellens, H., Siegel, D. P., Alford, D., Yeagle, P. L., Boni, L., Lis, L. J., Quinn, P. J., & Bentz, J. (1989) *Biochemistry 28*, 3692.
Gawrisch, K., Parsegian, V. A., Rand, R. P., Fuller, N., Tate, M. W., Hajduk, D., & Gruner, S. M. (1990) *Biophys. J. 57*, 35a.
Gmur, N. F., & White-Depace, S. M., Eds. (1986) *National Synchrotron Light Source Users Manual*, Brookhaven National Laboratory, Upton, NY.
Gruner, S. M. (1987) *Science 238*, 305–312.
Gruner, S. M., Milch, J. R., & Reynolds, G. T. (1982) *Rev. Sci. Instrum. 53*, 1770–1778.
Gruner, S. M., Rothschild, K. J., deGrip, W. J., & Clark, N. A. (1985) *J. Phys. (Paris) 46*, 193–201.
Gruner, S. M., Tate, M. W., Kirk, G. L., So, P. T. C., Turner, D. C., Keane, D. T., Tilcock, C. P. S., & Cullis, P. R. (1988) *Biochemistry 27*, 2853–2866.
Guinier, A. (1963) *X-ray Diffraction*, Freeman, San Francisco, CA.
Hui, S. W., Stewart, T. P., & Boni, L. T. (1983) *Chem. Phys. Lipids 33*, 113–126.
Laggner, P., Lohner, K., & Kuller, K. (1987) *Mol. Cryst. Liq. Cryst. 151*, 373–388.
Laggner, P., Kriechbaum, M., Rapp, G., & Hendrix, J. (1989) *2nd European Conference on Program in X-ray Synchrotron Radiation Research*, Rome, Italy.
Lis, L. J., & Quinn, P. J. (1991) *J. Appl. Crystallogr. 24*, 48–60.
Mencke, A. P., & Caffrey, M. (1991) *Biochemistry 30*, 2453–2463.
Milch, J. R. (1979) *IEEE Trans. Nucl. Sci. 26*, 338–345.
Milch, J. R., Gruner, S. M., & Reynolds, G. T. (1982) *Nucl. Instrum. Methods 201*, 43–52.
Quinn, P. J., & Lis, L. J. (1987) *J. Colloid Interface Sci. 115*, 220–224.
Ranck, J. C., Letellier, L., Shechter, E., Krop, B., Pernot, P., & Tardieu, A. (1984) *Biochemistry 23*, 4955–4961.
Seddon, J. M., Cevc, G., & Marsh, D. (1983) *Biochemistry 22*, 1280–1289.
Shyamsunder, E., Gruner, S. M., So, P. T. C., Turner, D. C., & Tate, M. W. (1988) *Biochemistry 27*, 2332–2336.
Siegel, D. P. (1984) *Biophys. J. 45*, 399–420.
Siegel, D. P. (1986a) *Biophys. J. 49*, 1155–1170.
Siegel, D. P. (1986b) *Biophys. J. 49*, 1171–1183.
Siegel, D. P. (1986c) *Chem. Phys. Lipids 42*, 279–301.

Siegel, D. P. (1987) in *Membrane Fusion* (Sowers, A. E., Ed.) Plenum, New York.
Siegel, D. P., & Banschbach, J. (1990) *Biochemistry 29*, 5975-5981.
Siegel, D. P., Burns, J. L., Chestnut, M. H., & Talmon, Y. (1989) *Biophys. J. 56*, 161.
Small, D. M. (1986) *The Physical Chemistry of Lipids*, Vol. 4. of Handbook of Lipid Research (Hanahan, D. J., Ed) Plenum, New York.
Tate, M. W. (1987) *Equilibrium and Kinetic States of the L_α-H_{II} Phase Transition*, Ph.D. Thesis, Princeton University, Princeton, NJ.
Tate, M. W., & Gruner, S. M. (1989) *Biochemistry 28*, 4245-4285.
Verkleij, A. J. (1984) *Biochim. Biophys. Acta 779*, 43-63.
Verkleij, A. J., van Echteld, C. J. A., Gerritsen, W. J., Cullis, P. R., & de Kruijff, B. (1980) *Biochim. Biophys. Acta 600*, 620-624.

Investigation of Anion Binding to Neutral Lipid Membranes Using ^2H NMR†

John R. Rydall and Peter M. Macdonald*

Department of Chemistry and Erindale College, University of Toronto, Toronto, Ontario, Canada M5S 1A1

Received June 14, 1991; Revised Manuscript Received October 15, 1991

ABSTRACT: The binding of aqueous anions (ClO_4^-, SCN^-, I^-, and NO_3^-) to lipid bilayer membranes composed of 1-palmitoyl-2-oleoyl-*sn*-glycero-3-phosphocholine (POPC) was investigated using deuterium (^2H) and phosphorus-31 (^{31}P) nuclear magnetic resonance (NMR) spectroscopy. The ability of these anions to influence the ^2H NMR quadrupole splittings of POPC, specifically labeled at the α or β position of the choline head group, increased in the order $NO_3^- \ll I^- < SCN^- < ClO_4^-$. In the presence of these chaotropic anions, the quadrupole splitting increased for α-deuterated POPC and decreased for β-deuterated POPC, indicating a progressive accumulation of negative charge at the membrane surface. Calibration of the ^2H NMR quadrupole splittings with the amount of membrane-bound anion permitted binding isotherms to be generated for perchlorate, thiocyanate, and iodide, up to concentrations of 100 mM. The binding isotherms were analyzed by considering electrostatic contributions, according to the Gouy-Chapman theory, as well as chemical equilibrium contributions. For neutral POPC membranes, we obtained ion association constants of 32, 80, and 115 M^{-1} for iodide, thiocyanate, and perchlorate, respectively. These values increase in the order expected for a Hofmeister series of anions. We conclude that the factor determining whether a particular anion will bind to lipid bilayers is the ease with which that anion loses its hydration shell. A comparison of the calibrated sensitivity of the ^2H NMR quadrupole splitting to these and other ligands indicated that, in addition to charge, two factors dictate the level of the ^2H NMR response: first, whether the ligand is cationic or anionic; and second, whether the ligand is predominantly hydrophobic or hydrophilic in nature. Both of these factors can be seen to arise from the details of the "choline-tilt" model of the ^2H NMR response to surface charges.

Ion binding to membrane surfaces represents a probable regulatory mechanism in biology (Hille, 1984). The polar groups of membrane lipids are involved in that they themselves contribute to the surface charge and in that they constitute ion-binding sites. It has been shown that phosphatidylcholines respond to the presence of bound ions and that this response can be detected using deuterium nuclear magnetic resonance (^2H NMR)[1] spectroscopy (Akutsu & Seelig, 1981; Altenbach & Seelig, 1984; Macdonald & Seelig, 1987a,b). Recent evidence indicates that this sensitivity of phosphatidylcholine involves a concerted conformational change of the choline head group, undergone in response to changes in the membrane surface charge. In this sense, phosphatidylcholine behaves like a "molecular voltmeter". Models of this conformational change suggest that the entire choline group tilts with respect to the plane of the membrane as its quaternary nitrogen is either attracted to or repelled by opposite or like surface charges (Scherer & Seelig, 1989; Roux et al., 1989; Macdonald et al., 1991).

In this report, we describe a detailed, comparative investigation of the binding of aqueous anions (ClO_4^-, SCN^-, I^-, NO_3^-) to neutral phosphatidylcholine membranes using ^2H NMR. We have determined ion-binding isotherms and extracted association constants by taking into account both electrostatic and equilibrium binding considerations. In addition, this comparison has delineated certain limitations of ^2H NMR for the investigation of such binding equilibria, while clarifying other aspects of the ^2H NMR response to surface charges.

† Supported by the National Science and Engineering Research Council of Canada.

* To whom correspondence should be addressed.

[1] Abbreviations: ^1H NMR, proton nuclear magnetic resonance; ^{31}P NMR, phosphorus-31 nuclear magnetic resonance; ^2H NMR, deuterium nuclear magnetic resonance; POPC, 1-palmitoyl-2-oleoyl-*sn*-glycero-3-phosphocholine; POPA, 1-palmitoyl-2-oleoyl-*sn*-glycero-3-phosphate; HEPES, *N*-(2-hydroxyethyl)piperazine-*N*'-2-ethanesulfonic acid; TLC, thin-layer chromatography; CSA, chemical shift anisotropy; DSC, differential scanning calorimetry.

0006-2960/92/0431-1092$03.00/0